Reac Kinet Mech Cat (2012) 107:405–419
DOI 10.1007/s11144-012-0477-6

Preferential oxidation of CO on Ni/CeO_2 catalysts in the presence of excess H_2 and CO_2

Sachin Malwadkar · Parthasarathi Bera · M. S. Hegde · C. V. V. Satyanarayana

Received: 29 February 2012 / Accepted: 26 June 2012 / Published online: 12 July 2012

Abstract Preferential oxidation of CO (CO-PROX) was carried out over Ni supported on CeO_2 prepared by the co-precipitation method. The influence of metal loadings (2.5, 5 and 10 wt.% Ni) and the reaction conditions such as reaction temperature and feed composition on CO oxidation and oxidation selectivity were evaluated by using dry reformate gas. No other reactions like CO or CO_2 methanation, coking, reverse water gas shift (RWGS) reaction is observed in the temperature range of 100–200 °C on these catalysts. Hydrogen oxidation dominates over CO oxidation above the temperature of 200 °C. An increase in oxygen leads to an increase in CO conversion but a simultaneous decrease in the O_2 selectivity. It has been noticed that 5 and 10 % Ni/CeO_2 show better catalytic activity towards CO-PROX reaction. These catalysts were characterized by S_{BET}, XRD, TEM, XPS and H_2-TPR.

Keywords Fuel cells · CO-PROX · Ni · CeO_2 · Methanation

Introduction

Fuel cells are viable alternative sources for clean energy generation. A variety of fuel cells for different applications are under different stages of development. Proton exchange membrane fuel cells (PEMFC) possess a series of advantageous

S. Malwadkar (✉) · C. V. V. Satyanarayana
Catalysis Division, CSIR-National Chemical Laboratory, Pune 411008, India
e-mail: sachin24ncl@gmail.com

P. Bera
Surface Engineering Division, CSIR-National Aerospace Laboratories, Bangalore 560017, India

M. S. Hegde
Solid State and Structural Chemistry Unit, Indian Institute of Science, Bangalore 560012, India

features that make them leading candidates, gaining popularity and commercial acceptability, as energy conversion devices, since they can produce power at much higher efficiencies with near zero emission [1]. However, PEMFCs require hydrogen feed that is mostly free from CO (<10 ppm), as otherwise the Pt based anode catalyst would be deactivated rapidly [2, 3]. However, typical gas mixtures that are produced from steam reforming or autothermal reforming contain CO in the range of 8–15 mol.% varying based on the exit temperature of the gas from the reformer. The gas composition also changes based on the primary fuel used for reforming. This high concentration of CO is brought down to less than 0.5 mol.%, through a two-stage water gas shift (WGS) reactor, in which CO is reacted with water to produce hydrogen and carbon dioxide. Since the CO level is still much higher than a PEMFC anode can tolerate, it has to be selectively oxidized to bring its concentration to below 10 ppm in excess of H_2, H_2O and CO_2, which is a current challenge in heterogeneous catalysis. This process is called preferential oxidation of CO (CO-PROX) [4–6], rather than selective oxidation as it is not possible to suppress H_2 oxidation completely. As the free energies of CO and H_2 oxidation reactions are very close (-281.4 kJ mol^{-1} for CO oxidation and -243.6 kJ mol^{-1} for H_2 oxidation), the catalyst used for this process has to preferentially oxidize CO in the presence of excess H_2, to prevent the loss of valuable hydrogen that is present in high concentrations (45–79 mol.%) in reformate streams. Generally, in industrial hydrogen production, CO_2 is first removed and subsequently the gas stream is cleansed of CO through methanation. However, it is not feasible to follow this method for small decentralized hydrogen generation units that are required for PEM fuel cells, due to cost and size factors. To use pressure swing adsorption, gas streams have to be pressurized, which in turn consume parasitic power and this can also lead to increased size (bulkiness) of the fuel processor.

A prime requirement of a good PROX catalyst is its high CO oxidation rate combined with high oxidation selectivity at low temperatures. The CO-PROX reaction has extensively been investigated recently [5–12]. However, in most of the studies, the reaction feeds used were not representative of typical reformate that exited from a low temperature WGS reactor (CO, CO_2, H_2, CH_4 and H_2O). The presence of some of the gas components in the mixture (typically water and CO_2) can alter the reaction rates, selectivity and in most cases, the catalyst life. For example, the gold supported on Fe_2O_3 or manganese oxides was found to be highly active at low temperature (<100 °C) for CO-PROX. However, the presence of CO_2 and water led to rapid deactivation of the catalyst [13]. It was reported that the presence of CO_2 led to the formation of carbonates, which are strongly held on to the support on these catalyst, thus leading to their deactivation.

Highly dispersed gold on reducible supports is a well known catalyst for CO oxidation and also this catalyst has gained attraction for the CO-PROX reaction [5, 6]. The mass-specific reaction rates on supported Au catalyst are high at 80 °C and even at lower temperature, as compared to standard PROX catalyst such as Pt/Al_2O_3 at their operating temperature of 150–200 °C [14]. But these catalysts have some drawbacks like a metal loading around 5 %, which is very high, they cannot stand high space velocity and they deactivate very fast in the presence of CO_2. On the other hand, on the Pt/Al_2O_3 catalyst, Korotkikh and Farrauto [15] reported that

though CO_2 could not affect CO oxidation, the presence of H_2O (steam) reduced CO oxidation by about 10 mol.%. Noble metal catalysts supported on oxides, reported so far, were not so selective, e.g. conventional Al_2O_3 supported Pt (Pt/Al_2O_3) required $\geq$2 vol.% O_2 to oxidize 1 vol.% CO in H_2 rich gas, though the stoichiometric requirement of O_2 is only 0.5 % ($CO + 1/2\ O_2 \rightarrow CO_2$) [15]. The rest of O_2 oxidizes valuable H_2 that could lead to a loss of H_2 even up to 3 mol.%. However, Pt catalysts were reported to offer better activity as well as stability, but most of the Pt based catalysts studied work at higher temperatures (>150 °C).

The well-known enhancement of the total oxidation activity of CuO when supported on oxides like CeO_2 has been attributed to a 'synergistic' effect [7, 16]. It is proposed that well dispersed metal on CeO_2, which is reducible at lower temperature with respect to bulk CuO, could easily adsorb CO. As a consequence, this catalyst exhibited high activity/selectivity for low temperature CO oxidation [17–19]. The information gained might aid the development of these catalysts, which would replace precious metal catalyst for low temperature CO oxidation. Additionally, it was demonstrated that the redox processes undergoing upon the CO oxidation involved the reduction and oxidation of both the copper and the ceria phases [20–23]. It was also postulated that the presence of copper enhances the redox behavior, the oxygen storage capacity and thermal stability of ceria [24]. However, the CO-PROX activity over other transition metals supported on CeO_2 such as Ni/CeO_2 lacks in the literature [5, 6]. In this paper, we report the CO-PROX by using feed composition more representative of the feed to PROX reactor in PEM fuel cell over Ni/CeO_2 catalysts prepared by the co-precipitation method and characterized by BET surface area (S_{BET}), powder X-ray diffraction (XRD), transmission electron microscopy (TEM), H_2-temperature programmed reduction (H_2-TPR), and X-ray photoelectron spectroscopy (XPS). Ni catalysts are widely applied for the methanation reaction, whereas in this work, we have tried selective oxidation of CO in the presence of hydrogen by adding small amount of oxygen in the reaction feed. Methanation of CO consumes three molecules of hydrogen per mole of CO and CO_2 from hydrogen rich reformate gas, leading to a loss of valuable hydrogen. In the present work, we have used nickel supported on high oxygen storage capacity support like ceria and tried to get the activity similar to that of copper based ceria catalyst.

Materials and methods

Preparation

Catalysts were prepared by the co-precipitation method with different loadings of nickel of 2.5, 5, 10 and 15 % on CeO_2 by using potassium hydroxide as a precipitating agent. Appropriate amounts of $Ni(NO_3)_2{\cdot}H_2O$, $Ce(NO_3)_3{\cdot}6H_2O$ and KOH were dissolved in distilled water to prepare 0.2 M solutions of each salt. The salt solution of nickel and ceria was precipitated by adding slowly into a 0.2 M solution of potassium hydroxide in the round bottom flask. The pH was maintained to 9.5–10 and the mixture was digested for 3 h at 80–90 °C. The precipitate was cooled to room temperature, filtered and washed with chlorine free water to remove

potassium ions from the final material. Then it was dried at 100 °C for 8 h and then this material was crushed and calcined at 500 °C for 5 h to get into oxide form. Metal concentrations in all catalysts were evaluated by inductively coupled plasma-atomic emission spectroscopy (ICP-AES) using Perkin Elmer P-1000 instrument.

Characterization

S_{BET} of the catalysts studied here were estimated from the N_2 adsorption–desorption isotherms measured at −196 °C and evacuated at 300 °C for 3 h prior to N_2 adsorption using NOVA-1200 instrument. XRD data of these catalysts were collected on Siemens D5005 diffractometer using CuK_α radiation (1.5418 Å). Data were obtained at a scan rate of 1° min^{-1} with 0.02° step size in the 2θ range of 10°–100°. A JEOL JEM-200CX transmission electron microscope operated at 200 kV was employed to carry out TEM studies. XPS of Ni/CeO_2 catalyst samples were recorded in an ESCA-3 Mark II spectrometer (VG Scientific Ltd., England) using AlK_α radiation (1,486.6 eV) run at 15 kV and 10 mA as X-ray source. Binding energies reported here were calculated with reference to C1s at 285 eV having a precision of ±0.2 eV. For XPS analysis, 8 mm diameter pellets of powder samples were mounted on the sample holder and kept into preparation chamber with ultrahigh vacuum (UHV) at 10^{-9} Torr for 5 h in order to desorb any volatile species present on the sample surface. After this time period, samples were placed into analyzer chamber with UHV at 10^{-9} Torr.

H_2-TPR experiments were performed using a Micromeritics AutoChem 2910 instrument. A weighed amount (0.5 g) of the sample was placed in a quartz reactor and treated with Ar at 500 °C for 2 h. A gas mixture of H_2 (5 %)–Ar (95 %) was then passed (30.22 cm^3 min^{-1}) through the reactor. The temperature was raised to 900 °C at a heating rate of 5 °C min^{-1}.

Catalytic activity test

CO-PROX reactions were performed in a fixed bed, down flow, glass reactor with inner diameter of 15 mm using 0.5 cm^3 of the calcined catalyst sandwiched between two glass-wool plugs. Pellets of the catalyst sample were made without using any binder and crushed to the sizes of 10–20 mesh. The sample was activated at 500 °C for 3 h in air to clean the surface of the catalyst and cooled to reaction temperature. A feed gas mixture of containing H_2 (74.05 %), CO (0.5 %), CH_4 (2.05 %), and CO_2 (23.40 %) was passed through a mass flow controller (Bronkhorst Hi Tech) at specified flow rates with GHSV of 10,000–30,000 h^{-1}. The desired amount of oxygen in the form of air ($O_2/CO = 0.5–2.0$) was sent accurately through a second mass flow controller. The product gas mixture was analyzed by using an online gas chromatograph (CHEMITO 8610) equipped with a methanator (Accessory of GC) to detect ppm levels of CO. A Spherocarb column of 8 feet length and 1/8 inch diameter was used to get clear separation of all gas components (H_2, O_2, N_2, CO, CH_4 and CO_2) using TCD and FID detectors. A certified standard gas mixture was used as a reference to estimate the concentration of gases. The gas chromatograph was also connected in series with an IR gas analyzer (Fuji Electric) for estimating

CO, CO_2, CH_4 and O_2 accurately. Methanation was evaluated from the amount of CH_4 detected in the feed, whereas CO and O_2 conversions and oxidation selectivity were calculated on the basis of O_2 and CO consumptions written as follows:

$$\text{CO Conversion (mol.\%)} = \frac{\text{mole of CO}_{\text{in}} - \text{mole of CO}_{\text{out}}}{\text{mole of CO}_{\text{in}}} \times 100$$

$$\text{O}_2\text{ Conversion (mol.\%)} = \frac{\text{mole of O}_{2\text{in}} - \text{mole of O}_{2\text{out}}}{\text{mole of O}_{2\text{in}}} \times 100$$

$$\text{Oxidation selectivity (mol.\%)} = \frac{\text{mole of CO}_{\text{in}} - \text{mole of CO}_{\text{out}}}{2(\text{mole of O}_{2\text{in}} - \text{mole of O}_{2\text{out}})} \times 100$$

Results and discussion

Characterization studies

Weight percentage values of Ni and Ce from chemical analysis as determined by ICP-AES are given in Table 1. S_{BET} values of the samples studied here are shown in the same table, which indicates increase in surface area from 63 for 2.5 % Ni/CeO_2 to 91 $m^2\ g^{-1}$ for 15 % Ni/CeO_2.

XRD patterns of 2.5, 5 and 10 % Ni/CeO_2 before and after the reaction are displayed in Fig. 1. The patterns could be indexed for CeO_2 with fluorite structure [25]. The lattice parameter (a) values are 5.4168, 5.4059 and 5.3688 Å for 2.5, 5 and 10 % Ni/CeO_2, respectively. The systematic decrease in lattice parameter values with an increase in Ni concentration could indicate the formation of a solid solution in the catalysts to certain extent suggesting the presence of Ni-CeO_2 interaction. A recent study of Ni/CeO_2 catalysts shows the formation of $Ce_{1-x}Ni_xO_{2-y}$ solid solution with a limit of solubility in the range of 10–12 % Ni [26]. In the same study, a trace amount of NiO could be observed when the Ni content is above 20 %. In our study, diffraction lines due to NiO could not be detected even when the NiO region (30–50°) was expanded for 10 % Ni/CeO_2. XRD patterns of Ni/CeO_2 catalysts after the reaction also do not show NiO related peaks (Fig. 1b). However, diffraction lines in all the catalysts are broad and crystallite sizes calculated by Debye–Scherrer method are in the range of 6–8 nm. There is no significant change in the particle sizes after the catalytic reaction.

Table 1 Metal percentage, specific surface area and H_2 consumption of several Ni/CeO_2 catalysts

Catalysts	Metal percentage (wt.%)[a]		S_{BET} ($m^2\ g^{-1}$)	H_2 consumption (mmol g^{-1})
	Ni	Ce		
2.5 % Ni/CeO_2	2.56	97.44	63.0	0.82
5 % Ni/CeO_2	5.09	94.04	67.0	0.95
10 % Ni/CeO_2	10.11	89.89	81.0	1.12
15 % Ni/CeO_2	14.50	84.50	91.0	1.62

[a] Chemical analysis results obtained from ICP-AES

TEM images of as-prepared 5 % Ni/CeO_2 and the same sample after the reaction are shown in Fig. 2. The morphology of CeO_2 crystallites in all the catalysts is cubic. The average size of CeO_2 crystallites in 5 % Ni/CeO_2 is 9 nm that agrees well with XRD studies. TEM images of catalyst are similar to pure CeO_2 image and there is no agglomerated NiO observed in case of Ni/CeO_2 crystalline surface. The ring type electron diffraction pattern of catalyst could be indexed to polycrystalline CeO_2 in fluorite structure and even after the reaction, no line or even diffraction spots corresponding to any of the oxides of Ni is detected (Fig. 2b). Therefore, TEM

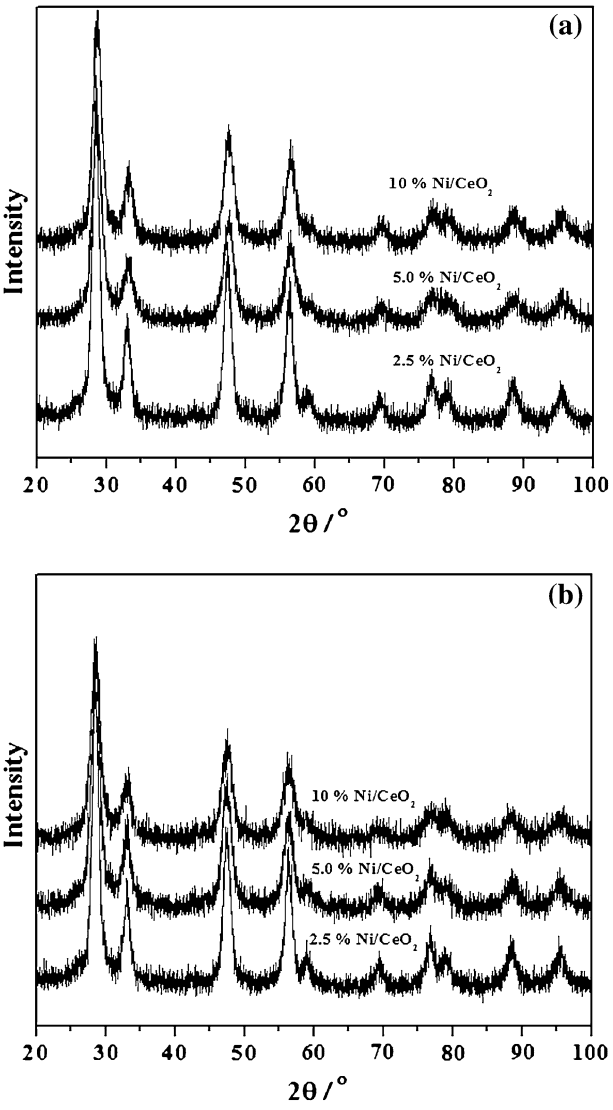

Fig. 1 XRD patterns of different Ni/CeO_2 catalysts of (**a**) before reaction and (**b**) after reaction

studies suggest that NiO is not separated out from CeO_2 support, may be finely dispersed on CeO_2 crystallites.

The XPS of Ni2p and Ce3d core levels in 5 % Ni/CeO_2 catalyst before and after CO-PROX reaction are shown in Fig. 3. The Ni2p core level region is given on the top of Fig. 3. $Ni2p_{3/2,1/2}$ peaks could be resolved into a set of spin–orbit doublet. Accordingly, $Ni2p_{3/2,1/2}$ peaks at 856.0 and 872.4 eV with a satellite peak at 7 eV bellow the main peak and spin–orbit separation of 16.4 eV could only be assigned to Ni in the +2 oxidation state [27, 28]. Satellite peaks are characteristic of oxidized transition metals, especially Fe, Co, Ni and Cu [29]. It is well documented that an additional excitation of a second electron occurs during the emission of a photoelectron of a core level creating a hole in the core level. The sudden creation of a hole in $Ni2p^6$ filled orbital from Ni^{2+} ion present in the catalyst makes Ni^{3+} ion and it becomes unstable. Therefore, an electron transfer from O2p level to Ni3d level occurs that leads to satellite peaks in the Ni2p core level spectrum as seen in Fig. 3 that is marked by a *. Ce3d core level spectra obtained from 5 % Ni/CeO_2 catalysts before and after the reaction are shown in the bottom of Fig. 3. $Ce3d_{5/2,3/2}$ peaks at 882.5 and 900.9 eV with satellite features (* marked in the figure) correspond to CeO_2 with Ce^{4+} oxidation state [30]. Satellites in Ce3d level in CeO_2 at 888.6, 898.7, 906.6 and 916.8 eV marked in the spectra are well characterized in the literature [31–34]. Thus, the characteristic spectra of Ni2p and Ce3d in Ni/CeO_2 catalyst confirm that Ni and Ce are in +2 and +4 oxidation states, respectively. However, the possibility of the presence of a small amount of Ce^{3+} on the surface level could not be ruled out. It is also important to note that there is no significant change in the spectral envelops and peak positions of Ni2p and Ce3d after CO-PROX reaction. This indicates that oxidation states of Ni and Ce in Ni/CeO_2 catalysts have not been changed during the reaction. The relative surface concentrations of Ni and Ce in 5 % Ni/CeO_2 catalyst have been estimated by the relation [35, 36]:

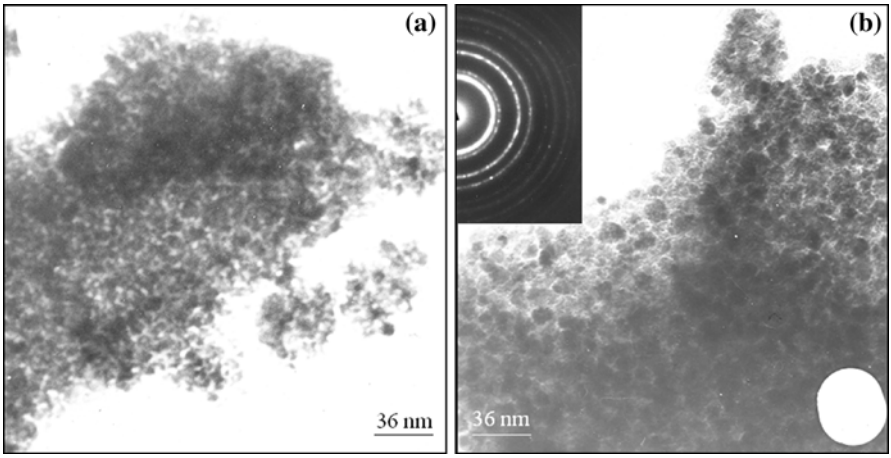

Fig. 2 TEM images of 5 % Ni/CeO_2 catalyst of (**a**) before reaction and (**b**) after reaction

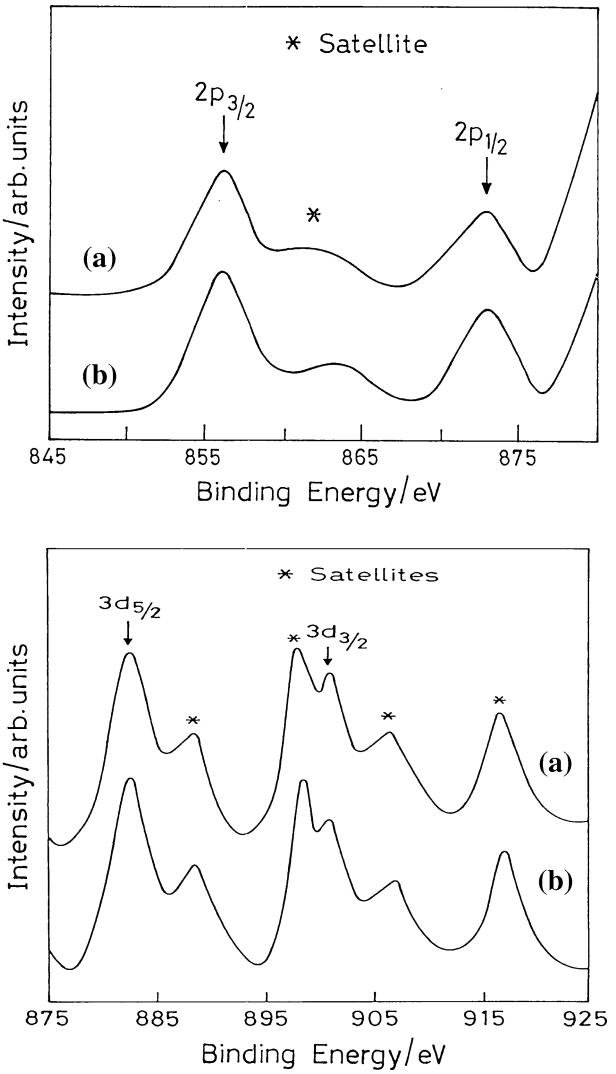

Fig. 3 *Top* XPS of Ni2p of 5 % Ni/CeO_2 catalyst of (*a*) before reaction and (*b*) after reaction, *Bottom* XPS of Ce3d of 5 % Ni/CeO_2 of (*a*) before reaction and (*b*) after reaction

$$\frac{C_{Ni}}{C_{Ce}} = \frac{I_{Ni}\,\sigma_{Ce}\,\lambda_{Ce}\,D_{Ce}}{I_{Ce}\,\sigma_{Ni}\,\lambda_{Ni}\,D_{Ni}}$$

where C, I, σ, λ and D are the surface concentration, intensity, photoionization cross-section, mean escape depth and analyzer detection efficiency. Integrated intensities of Ni2p and Ce3d peaks have been taken into account to estimate the surface concentration, whereas photoionization cross-sections and mean escape depths have been obtained from the literature [37, 36]. The analyzer detection efficiency that is called geometric factor was taken as 1, because the maximum

intensity in this spectrometer is obtained at 90°. Thus, the calculated surface concentration of Ni is 32 % in 5 % Ni/CeO_2 catalyst indicating that the surface concentration of Ni is 4–6 times higher than what is taken in preparation that suggests surface segregation of Ni^{2+} ions on CeO_2 surface.

H_2-TPR studies

The H_2-TPR profiles of different Ni/CeO_2 catalysts are shown in Fig. 4. From the TPR profile, it is clear that the reducibility of Ni^{2+} species is modified in the presence of CeO_2. The low Ni loaded CeO_2 catalysts shows one intense reduction peak along with a weak peak, whereas multiple peaks could be observed in the catalysts with high Ni loadings indicating the existence of more than one Ni^{2+} species in the catalysts. In all cases, the presence of broad peak envelopes from 150 to 500 °C for H_2 consumption could indicate the reduction of well dispersed NiO particles on CeO_2 matrix. The low temperature reduction peak at 270 °C with a low temperature tail in the 2.5 % Ni/CeO_2 catalyst is due to the reduction of finely dispersed and weakly held NiO particles on CeO_2 surface and a small hump at 520 °C is attributed to initial surface reduction of CeO_2 according to the literature [38]. The reduction of these fine NiO particles occurs at lower temperature compared to bulk NiO reduction reported in the literature [39]. On the other hand, peaks located in the region of 250–500 °C in the cases of Ni/CeO_2 catalysts with higher amounts of Ni could be ascribed to the reduction of larger bulk NiO and incorporated Ni^{2+} cations into CeO_2 fluorite structure [26, 40]. A decrease in the reduction temperature of finely dispersed NiO particles is seen to be further lowered to 225 °C with an increase in Ni concentration. The observed high temperature reduction peak above 400 °C in the catalysts with high Ni concentrations could

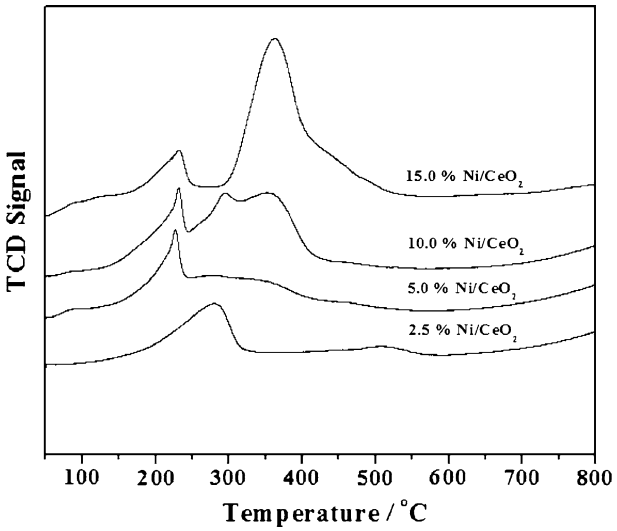

Fig. 4 H_2-TPR profiles of different Ni/CeO_2 catalysts

demonstrate the strong interaction between Ni^{2+} and CeO_2 through $–Ni^{2+}–O^{2-}–Ce^{4+}$-interfacial networks that agrees well with the literature [26, 40]. The presence of a very weak Ni-CeO_2 interaction peak in low Ni loaded catalyst could suggest a limited Ni integration into the fluorite lattice, which could be substantiated from calculated lattice parameter values of these catalysts. The peak at 368 °C observed in the catalysts with high Ni contents could be attributed to the reduction of larger bulk NiO particles [40]. As the amount of bulk NiO particles is more in the 15 % Ni/CeO_2 catalyst, this peak appears to be more intense in the 15 % Ni/CeO_2 catalyst in relation to other catalysts with lower Ni contents. Consequently, the envelope of the TPR profile is broadest in 15 % Ni/CeO_2. Therefore, the observed total H_2 consumption of 1.62 mmol g^{-1} (Table 1) is the highest in 15 % Ni/CeO_2 among all the catalysts and a major fraction of this H_2 consumption is due to reduction of larger bulk NiO particles. A small H_2 consumption peak at 520 °C due to CeO_2 support is hidden with higher Ni loadings, because the external surface of CeO_2 is significantly lowered by the presence of Ni. However, in all catalysts, a tail with increasing intensity is observed after 700 °C, which could be assigned for bulk reduction of CeO_2 [38].

CO-PROX activity studies

Catalytic activity evaluation of nickel-loaded ceria was carried out at the realistic conditions of fuel cells. For the whole study, the O_2/CO ratio was kept at 1, which was more than that of required for the oxidation of CO to achieve better CO conversion with space velocity 10,000 h^{-1}. Fig. 5 shows the CO conversion, O_2 conversion and oxidation selectivity with respect to temperature for the series of Ni/CeO_2 catalysts at 100–250 °C. From the studied catalysts, 5 and 10 % Ni/CeO_2 show better CO oxidation activity as compared with other catalysts, whereas the CO-PROX activity is only substantially lower over ceria [41]. The maximum CO conversion is observed at temperatures around 200 °C in 5 and 10 % Ni/CeO_2, and complete oxygen conversion occurs at temperatures higher than 200 °C. It has also to be noted that the 15 % Ni/CeO_2 catalyst shows the lowest CO conversion. CO and O_2 conversion in 5 and 10 % Ni/CeO_2 behave similarly in the temperature range between 100 and 200 °C, but above 200 °C, the hydrogen oxidation reaction becomes much more prominent leading to a decrease in CO conversion and oxidation selectivity. Two regions could be differentiated in the catalytic activity profiles. In the first, the low temperature region, the competition between CO and H_2 for active oxygen species is relatively weak. The second region corresponds to points above maximum CO conversion where CO and H_2 strongly compete for available active oxygen that results decrease in oxidation selectivity.

The effect of excess oxygen on CO conversion and oxidation selectivity has also been studied on 5 % Ni/CeO_2 catalyst at temperature 200 °C with a space velocity of 10,000 h^{-1}, which is shown in Fig. 6. CO and H_2 oxidation are the only reactions that take place under the examined conditions. CO conversion increases with an increase in oxygen in the feed. However, a parallel decrease in the oxidation selectivity is observed due to hydrogen oxidation, because the hydrogen oxidation is favored in the presence of a large excess of oxygen. Added excess oxygen is

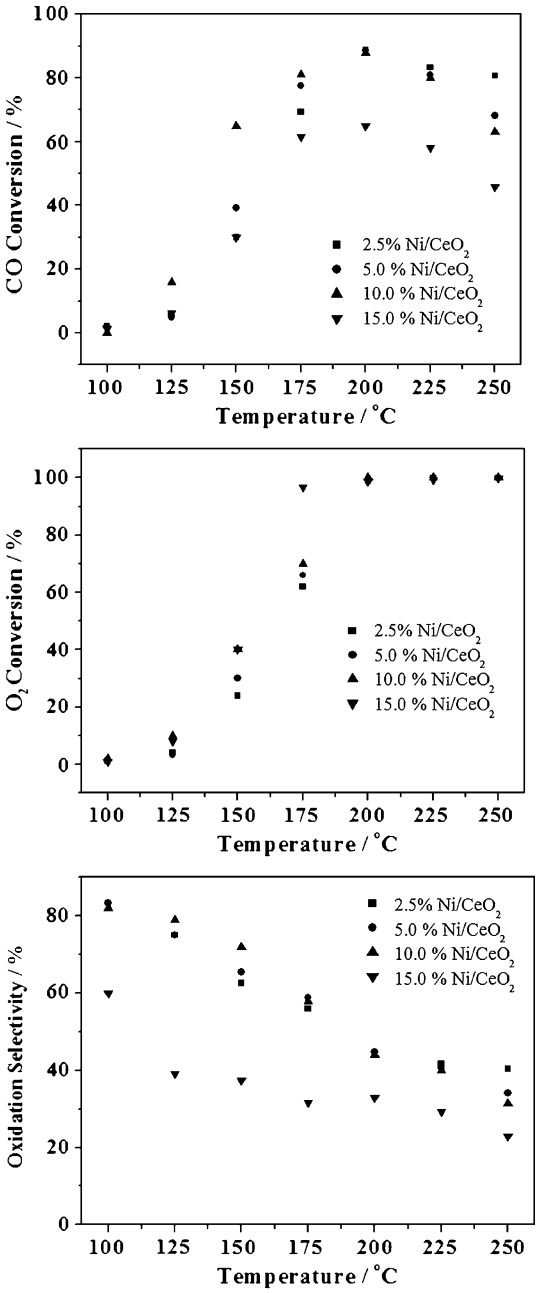

Fig. 5 CO-PROX reactions over several Ni/CeO_2 catalysts with respect to temperature

consumed completely for the hydrogen oxidation. It has also been reported that ceria acts as an oxygen buffer. As a result, the oxygen concentration over the catalyst would be constant up to certain oxygen inlet concentration when the maximum oxygen storage capacity of ceria is exceeded [41]. However, possible

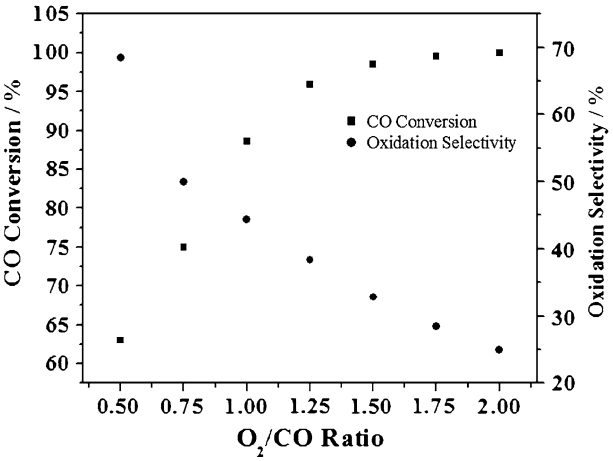

Fig. 6 Effect of excess oxygen on CO conversion and oxidation selectivity at 200 °C over 5 % Ni/CeO_2 catalyst

blockage of active sites for CO adsorption on the catalyst surface due to excess O_2 [42] does not occur on 5 % Ni/CeO_2 catalyst studied here. So, CO oxidation activity has not been affected by excess O_2.

Ni catalysts are also known to form CH_4 through the methanation of CO and CO_2 ($CO + 3\ H_2 \rightarrow CH_4 + H_2O$ and $CO_2 + 4H_2 \rightarrow CH_4 + 2H_2O$) and, consequently, the amount of hydrogen produced is reduced by the overall process [40, 43–45]. Nevertheless, for our catalyst, not even traces of methane are detected at the reactor outlet at temperature range of 100–200 °C analyzed. But a small amount of methanation is observed above 200 °C as shown in Fig.7, which is carried out with only dry reformate gas in the absence of oxygen. Generally, CO methanation occurs at a lower temperature, whereas CO_2 methanation is known to happen at higher temperature [43, 45]. This behavior is generally ascribed to the stronger interaction of CO with the surface of the catalyst compared to CO_2. There is CO conversion of 87.6 % at 250 °C over the 5 % Ni/CeO_2 catalyst, which corresponds to CO methanation, but it decreases with an increase in the temperature, which might be due to CO_2 methanation at higher temperature. CHN analysis of the catalyst after the reaction was also carried out and it has been found that there is no formation of coke. Hence, the CO-PROX activity over Ni/CeO_2 catalysts demonstrates that CO oxidation in the presence of excess hydrogen occurs selectively and there is a formation of trace amounts of CH_4 through methanation at higher temperature in the absence of O_2. It is also important to note that the presence of CO_2 in the feed stream leads to the reverse water gas shift (RWGS) reaction ($CO_2 + H_2 \rightarrow CO + H_2O$) in principle. However, the reverse water gas shift reaction is not observed over Ni/CeO_2 catalysts investigated here.

In the present study, catalysts with 5 and 10 wt.% Ni loadings shows best catalytic activity towards CO-PROX reaction among all the catalysts. The superior performance of these catalysts could be attributed to the higher fraction of finely

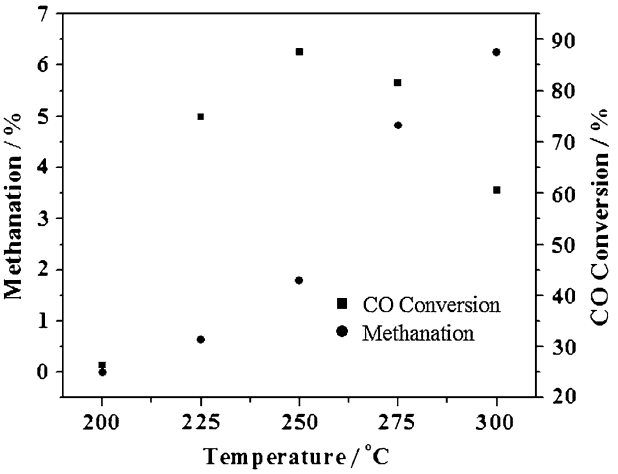

Fig. 7 Methanation over 5 % Ni/CeO_2 catalyst

dispersed and easily reducible NiO species interacting with CeO_2 support, which are the active phases for the catalysis. In the case of the 15 % Ni/CeO_2 catalyst, Ni is in excess on the CeO_2 support forming larger bulk NiO particles which have negligible interaction with CeO_2. TPR studies demonstrate that H_2 consumption over 15 % Ni/CeO_2 is the highest among all catalysts, but it is practically less active for the CO-PROX reaction. The reduction of larger bulk NiO particles present in huge amount on the 15 % Ni/CeO_2 surface has a major contribution for its very high H_2 consumption. Again, bulk CeO_2 and NiO are inactive for CO oxidation also. Hence, this low catalytic activity of 15 % Ni/CeO_2 catalyst compared to other Ni/CeO_2 catalysts is due to the presence of higher amounts of larger bulk NiO particles.

Conclusions

The CO-PROX was carried out in the presence of excess hydrogen over different loadings of Ni on CeO_2. CeO_2 with high oxygen storage capacity was used as a support to get better dispersion with high surface area. An increase in surface area is observed with an increase in nickel content. The XRD studies show the formation of a solid solution and crystallite sizes are in the range of 6–8 nm, which agrees well with TEM studies. XPS studies demonstrate that Ni and Ce are in +2 and +4 oxidation states in Ni/CeO_2 catalysts and there is no change in Ni^{2+} and Ce^{4+} states after the reaction. The surface concentration of Ni is 32 % in 5 % Ni/CeO_2, which is 4–6 times more what is taken in preparation indicating surface segregation of Ni^{2+} ions on CeO_2 surface. CeO_2 containing 5 and 10 % Ni shows low temperature activity towards CO-PROX reaction. Except the hydrogen oxidation, no other reaction like methanation, coking or reverse water gas shift reaction is observed on these catalysts. In the absence of oxygen, it shows a little methanation activity. An

increase in excess oxygen leads to a positive impact on CO conversion but O_2 selectivity is observed to decrease. In our case, the best result is observed at O_2/CO ratio of 2 with 99.94 % conversion and 24.98 % selectivity.

Acknowledgments SM and MSH are thankful to Council of Scientific and Industrial Research, Government of India for the award of Senior Research Fellowship and Emeritus Scientist Fellowship, respectively.

References

1. Appleby AJ, Foulkes FR (1989) Fuel cell handbook. Van Nostrand Reinhold, New York
2. Zalc JM, Löffler DG (2002) J Power Sources 111:58
3. Lemons RA (1990) J Power Sources 29:251
4. Lee SH, Han J, Lee K-Y (2002) J Power Sources 109:394
5. Mishra A, Prasad R (2011) Bull Chem React Eng Catal 6:1
6. Bion N, Epron F, Moreno M, Mariño F, Durprez D (2008) Top Catal 51:76
7. Avgouropoulos G, Ioannides T, Papadopoulou Ch, Batista J, Hocevar S, Matralis HK (2002) Catal Today 75:157
8. Grisel RJH, Nieuwenhuys BE (2001) J Catal 199:48
9. Schubert MM, Plzak V, Garche J, Behm RJ (2001) Catal Lett 76:143
10. Han Y-F, Kahlich MJ, Kinne M, Behm RJ (2002) Phys Chem Chem Phys 4:389
11. Kim DH, Lim MS (2002) Appl Catal A 224:27
12. Davran-Candan T, Demir M, Yildirim R (2011) Reac Kinet Mech Cat 104:389
13. Luengnaruemitchai A, Thoa DTK, Osuwan S, Gulari E (2005) Int J Hydrogen Energy 30:981
14. Schubert MM, Kahlich MJ, Gasteiger HA, Behm RJ (1999) J Power Sources 84:175
15. Korotkikh O, Farrauto R (2000) Catal Today 62:249
16. Wang JB, Shih W-H, Huang T-J (2000) Appl Catal A 203:191
17. Xiaoyuan J, Guanglie L, Renxian Z, Jianxin M, Yu C, Xiaoming Z (2001) Appl Surf Sci 173:208
18. Luo M-F, Zhong Y-J, Yuan X-X, Zheng X-M (1997) Appl Catal A 162:121
19. Ratnasamy P, Srinivas D, Satyanarayana C, Manikandan P, Kumaran RSS, Sachin M, Shetti VN (2004) J Catal 221:455
20. Martínez-Arias A, Fernandez-García M, Soria J, Conesa JC (1999) J Catal 182:367
21. Martínez-Arias A, Fernández-García M, Gálvez O, Coronado JM, Anderson JA, Conesa JC, Soria J, Munuera G (2000) J Catal 195:207
22. Wang JB, Lin S-C, Huang T-J (2002) Appl Catal A 232:107
23. Jernigan GG, Somorjai GA (1994) J Catal 147:567
24. Kacimi S, Barbier J Jr, Taha R (1993) Catal Lett 22:343
25. JCPDS, PDF No. 34-0394, ICDD
26. Barrio L, Kubacka A, Zhou G, Estrella M, Martínez-Arias A, Hanson JC, Fernández-García M, Rodriguez JA (2010) J Phys Chem C 114:12689
27. Navarro RM, Álvarez-Galván MC, Rosa F, Fierro JLG (2006) Appl Catal A 297:60
28. Lu Y, Xue J, Yu C, Liu Y, Shen S (1998) Appl Catal A 174:121
29. Hüfner S (2003) Photoelectron spectroscopy principles and applications, 3rd edn. Springer, Berlin, p 109
30. Sarma DD, Hegde MS, Rao CNR (1981) J Chem Soc, Faraday Trans 2 77:1509
31. Damyanova S, Pawelec B, Arishtirova K, Martinez Huerta MV, Fierro JLG (2008) Appl Catal A 337:86
32. Mullins DR, Overbury SH, Huntley DR (1998) Surf Sci 409:307
33. Bêche E, Charvin P, Perarnau D, Abanades S, Flamant G (2008) Surf Interface Anal 40:264
34. Huang J, Kang Y, Yang T, Wang Y, Wang S (2011) Reac Kinet Mech Cat 104:149
35. Powell CJ, Larson PE (1978) Appl Surf Sci 1:186
36. Penn DR (1976) J Electron Spectrosc Relat Phenom 9:29
37. Scofield JH (1976) J Electron Spectrosc Relat Phenom 8:129
38. Trovarelli A (1996) Catal Rev Sci Eng 38:439

39. Gonzalez-Delacruz VM, Ternero F, Pereñíguez R, Caballero A, Holgado JP (2010) Appl Catal A 384:9
40. Ocampo F, Louis B, Roger A-C (2009) Appl Catal A 369:90
41. Mariño F, Descorme C, Durprez D (2005) Appl Catal B 58:175
42. Kunkalekar RK, Salker AV (2012) Reac Kinet Mech Cat 106:395
43. Habazaki H, Yamasaki M, Zhanga B-P, Kawashima A, Kohno S, Takai T, Hashimoto K (1998) Appl Catal A 172:131
44. Takenaka S, Shimizu T, Otsuka K (2004) Int J Hydrogen Energy 29:1065
45. Krämer M, Stöwe K, Duisberg M, Müller F, Reiser M, Sticher S, Maier WF (2009) Appl Catal A 369:42